Title: Dysregulated alveolar epithelial cell progenitor function and identity in Hermansky-Pudlak syndrome pulmonary fibrosis

Authors: Joanna Y. Wang[1], Nigel S. Michki[2,3], Sneha Sitaraman[3], Brandon J. Banaschewski[3], Susan M. Lin[1,4], Jeremy B. Katzen[1,4], Maria C. Basil[1,4,5], Edward Cantu[6], Jarod A. Zepp[3,4], David B. Frank[2,3,4,5], and Lisa R. Young[1,3,4]

Author affiliations: [1]Division of Pulmonary, Allergy, and Critical Care, Department of Medicine, Perelman School of Medicine, University of Pennsylvania, Philadelphia, Pennsylvania, [2]Division of Cardiology, Department of Pediatrics, Children's Hospital of Philadelphia, Philadelphia, Pennsylvania, and [3]Division of Pulmonary and Sleep Medicine, Department of Pediatrics, Children's Hospital of Philadelphia, Philadelphia, Pennsylvania, [4]Lung Biology Institute, University of Pennsylvania, Philadelphia, Pennsylvania, [5]Penn Cardiovascular Institute, University of Pennsylvania, Philadelphia, Pennsylvania, [6]Department of Surgery, Perelman School of Medicine, University of Pennsylvania, Philadelphia, Pennsylvania.

Corresponding author: Lisa R. Young, M.D., Children's Hospital of Philadelphia, Leonard and Madlyn Abramson Pediatric Research Center, 3615 Civic Center Blvd, 4th Floor, Suite 416, Philadelphia, PA 19104. Phone: 215-590-3749, fax 215-590-3500, email: youngL5@chop.edu.

Conflict of interest: The authors have declared that no conflict of interest exists.

Brief summary: Impaired proliferation and aberrant transdifferentiation with emergence of a transitional cell state in alveolar epithelial cells in murine models of Hermansky-Pudlak syndrome pulmonary fibrosis

Abstract

Hermansky-Pudlak syndrome (HPS) is a genetic disorder associated with pulmonary fibrosis in specific subtypes, including HPS-1 and HPS-2. Single mutant HPS1 and HPS2 mice display increased fibrotic sensitivity while double mutant HPS1/2 mice exhibit spontaneous fibrosis with aging, which has been attributed to HPS mutations in alveolar epithelial type II (AT2) cells. Unifying mechanisms of AT2 cell dysfunction in genetic and sporadic fibrotic lung diseases remain unknown. Incorporating AT2 cell lineage tracing in HPS mice, we observed a progressive decline in AT2 cell numbers with aging and aberrant differentiation with increased AT2-derived alveolar epithelial type I cells. HPS AT2 cell proliferation was impaired *ex vivo* and *in vivo*, suggesting an intrinsic progenitor defect. Transcriptomic analysis of HPS AT2 cells revealed elevated expression of genes associated with aberrant differentiation and cellular senescence. Through lineage tracing and organoid modeling, we demonstrated that HPS AT2 cells were primed to persist in a $Krt8^{+}$ reprogrammed transitional state, mediated by p53 activity. These findings suggest that pulmonary fibrosis in HPS may be driven by AT2 cell progenitor dysfunction in the setting of p53-mediated senescence, highlighting a novel potential therapeutic target in HPS and suggesting unifying mechanisms underlying HPS and other forms of pulmonary fibrosis.

Introduction

Pulmonary fibrosis, characterized by the replacement of lung tissue with scar and destruction of lung architecture, is the end-stage manifestation of many respiratory diseases. Evidence suggests that dysfunctional alveolar epithelial type II (AT2) cells, which produce and store surfactant and act as progenitor cells in the alveolus, drive fibrotic remodeling (1-3). Numerous mechanisms of AT2 cell dysfunction have been identified, including accelerated senescence, which was first detected in telomere disorders, and increased endoplasmic reticulum (ER) stress, identified initially in pulmonary fibrosis due to surfactant protein C gene mutations (4-6). These mechanisms of cellular dysfunction in genetic forms of pulmonary fibrosis, in addition to mitochondrial dysfunction and apoptosis, have subsequently been observed in sporadic idiopathic pulmonary fibrosis (IPF) (4, 5, 7, 8).

Hermansky-Pudlak syndrome (HPS) is an autosomal recessive disorder of endosomal protein trafficking. The primary cause of mortality in certain subtypes of HPS is progressive pulmonary fibrosis, typically presenting in young adulthood in HPS-1 and HPS-4, and in childhood in HPS-2 (9). Notably, pulmonary fibrosis has not been observed in the other subtypes of HPS, including HPS-3. We originally demonstrated that HPS mutations specifically in the alveolar epithelium underlie fibrotic susceptibility, and studies from several groups have implicated apoptosis, impaired autophagy, and mitochondrial dysfunction in AT2 cells as potential contributing pathways (10-14). Despite these advances, the development of effective, targeted therapies for HPS-related pulmonary fibrosis (HPS-PF) has been limited by an incomplete understanding of the targetable mechanisms underlying HPS AT2 cell dysfunction. In addition, it remains unclear whether there are common final pathways of AT2 cell dysfunction shared across sporadic and genetic fibrotic lung diseases to inform the generalizability of therapies for pulmonary fibrosis that are currently available and those in development.

In this study, we examined HPS AT2 cells with aging to characterize the cellular and molecular mechanisms that drive AT2 cell dysfunction and their contribution to the fibrotic response. We utilized the double mutant HPS1/2 murine model, which exhibits spontaneous progressive fibrosis with aging, as well as the single mutant HPS1 and HPS2 models, which best reflect human disease genetics while

exhibiting fibrotic sensitivity without spontaneous fibrosis (13, 15-17). We show dysregulated maintenance of the alveolar epithelium in HPS, with loss of AT2 cells with aging in HPS1, HPS2, and HPS1/2 mice driven by aberrant differentiation and reduced proliferation. These impairments in AT2 cell progenitor function in HPS are brought about in part by p53-mediated senescence and result in the persistence of a Krt8^{+} reprogrammed transitional cell state. Our findings reveal a novel therapeutic target in HPS-PF and suggest the existence of shared mechanisms of disease between HPS and other sporadic and genetic fibrotic lung diseases.

Results

Loss of AT2 cells with aging in HPS mice

We first confirmed that double mutant HPS1/2 mice developed spontaneous, progressive fibrosis with aging as previously described (**Supplemental Figure 1A-D**) (16-18). We then utilized immunofluorescence (IF) for the AT2 cell marker, proSP-C, and the alveolar epithelial type I (AT1) cell marker, AGER, to examine the alveolar epithelium in aged HPS1/2 mice compared to wild type (WT) at 48 weeks of age. In addition to clusters of AT2 cell hyperplasia, we observed regions of near total proSP-C^{+} AT2 cell loss in HPS1/2 mice (**Figure 1A**). To measure AT2 cell numbers with aging *in situ*, AT2 cells in WT and HPS1/2 mice at 4, 8, 24, and 48 weeks of age were quantified via IF for proSP-C (**Figure 1B, C**). Starting at 8 weeks of age, we found a significant decrease in the percentage of proSP-C^{+} AT2 cells per total DAPI positive cells in HPS1/2 mice, with 10.3 ± 0.4% in HPS1/2 mice compared to 13.9 ± 0.3% in WT (adjusted $p = .02$). These percentages corresponded to a mean 31.0 ± 10.2 cells per high powered field (hpf) in HPS1/2 mice and 56.8 ± 10.4 AT2 cells per hpf in WT mice ($p < .0001$). There was progressive loss of AT2 cells with aging in HPS1/2 mice, which exhibited 8.1 ± 0.5% proSP-C^{+} cells at 48 weeks of age (adjusted $p = .001$), as well as WT mice with aging, with 11.5 ± 0.2% at 48 weeks of age (adjusted $p = .002$).

Significant AT2 cell loss with aging was also seen in single mutant HPS1 and HPS2 mice, by 8 weeks and 24 weeks of age, respectively (**Figure 1B, C**). At 8 weeks of age, HPS1 mice exhibited 12.1 ±

0.3% proSP-C$^+$ cells compared to 13.9 ± 0.3% in WT (adjusted p = .029); by 24 weeks of age, HPS2 mice displayed 9.3 ± 0.4% compared to 13.3 ± 0.3% in WT (adjusted p = .016). There was also progressive loss of AT2 cells over 48 weeks in HPS1 mice (adjusted $p < .0001$) and HPS2 mice (adjusted p = .037). To account for the possibility of immune cells and other cell types present in HPS mice that could alter the total cell count and contribute to lower percentages of proSP-C$^+$ cells, we quantified the percentage of proSP-C$^+$ cells per total epithelial cells as denoted by Nkx2.1 staining (**Supplemental Figure 2A-D**). There was a significant decrease in the percentage of proSP-C$^+$, Nkx2.1$^+$ cells in HPS1 compared to WT mice at 8 weeks of age (72.2 ± 3.2% vs. 78.2 ± 3.5, p = .046) and in HPS2 compared to WT mice at 24 weeks of age (65.0 ± 2.4% vs. 76.1 ± 3.9%, p = .0029) (**Supplemental Figure 2A-D**). In contrast, in HPS3 mice, a subtype not associated with pulmonary fibrosis, AT2 cell numbers were comparable to WT at 8 and 24 weeks of age (**Supplemental Figure 3A, B**). Furthermore, in transgenic epithelial-corrected HPS2 (HPS2 TG) mice, AT2 cell numbers were significantly increased compared to HPS2 mice at 24 weeks of age (**Supplemental Figure 3A, C**). No TUNEL-positive apoptotic AT2 cells were detected in WT or HPS mice across the same timepoints (**Supplemental Figure 4A**). Together, these data show that there is age-dependent accelerated and progressive loss of AT2 cells in HPS1, HPS2, and HPS1/2 mice, the HPS subtypes associated with fibrotic susceptibility.

Lineage tracing of HPS AT2 cells reveals spontaneous transdifferentiation

To confirm loss of AT2 cells based on proSP-C expression and investigate the etiology of AT2 cell loss by evaluating cell fate, we generated WT, HPS1, HPS2, and HPS1/2 Sftpc$^{CreERT2/+}$;R26R$^{EYFP/+}$ mice to perform lineage tracing of AT2 cells. Recombination with tamoxifen was induced at four weeks of age, prior to the timepoint where we observed onset of significant AT2 cell loss based on proSP-C immunostaining (**Figure 2A**). Quantification of the number of lineage-labeled AT2 cells (EYFP$^+$) in paraffin-embedded sections confirmed significant loss of AT2 cells starting at 8 weeks of age. HPS1/2 Sftpc$^{CreERT2/+}$;R26R$^{EYFP/+}$ mice exhibited 9.0 ± 0.8% lineage-labeled AT2 cells compared to 14.4 ± 0.8% in WT Sftpc$^{CreERT2/+}$;R26R$^{EYFP/+}$ mice (adjusted $p < 0.001$) (**Figure 2B**; **Supplemental Figure 5A**). Loss of

lineage-labeled AT2 cells was also seen in HPS1 Sftpc$^{CreERT2/+}$;R26R$^{EYFP/+}$ mice (11.8 ± 0.2% EYFP^{+} cells, adjusted p = .003) and HPS2 Sftpc$^{CreERT2/+}$;R26R$^{EYFP/+}$ (12.9 ± 1.1% EYFP^{+} cells, adjusted p = .034) compared to WT Sftpc$^{CreERT2/+}$;R26R$^{EYFP/+}$ mice (**Figure 2B**; **Supplemental Figure 5A**).

In HPS1/2 Sftpc$^{CreERT2/+}$;R26R$^{EYFP/+}$ mice, we observed the emergence of lineage-labeled cells that did not express proSP-C (EYFP^{+}, proSP-C^{neg}), constituting 7.4 ± 1.8% of all lineage-labeled cells at 8 weeks of age and 10.6 ± 0.5% at 24 weeks of age (**Figure 2C; Supplemental Figure 5A**). In contrast, EYFP^{+}, proSP-C^{neg} cells were not identified in WT, HPS1, or HPS2 Sftpc$^{CreERT2/+}$;R26R$^{EYFP/+}$ mice at 8 or 24 weeks of age (**Figure 2C; Supplemental Figure 5A**). To further evaluate AT2-to-AT1 cell transdifferentiation as an etiology of AT2 cell loss and account for the squamous morphology of AT1 cells, we performed immunostaining of thicker 150 μm whole mount lung sections. This revealed lineage-labeled EYFP^{+}, AGER^{+}, LAMP3^{neg} cells with the squamous morphology of AT1 cells in HPS1, HPS2, and HPS1/2 Sftpc$^{CreERT2/+}$;R26R$^{EYFP/+}$ mice, starting at 8 weeks of age (**Figure 2D**). No lineage-labeled AT1 cells were detected in WT Sftpc$^{CreERT2/+}$;R26R$^{EYFP/+}$ mice at 8 or 24 weeks of age (**Figure 2D**). These EYFP^{+} cells were likely not captured in HPS1 and HPS2 mice on thinner paraffin-embedded sections given the expansive, squamous morphology of AT1 cells. Notably, cuboidal lineage-labeled EYFP^{+}, AGER^{neg}, LAMP3^{neg} cells were also observed, only in HPS1/2 Sftpc$^{CreERT2/+}$;R26R$^{EYFP/+}$ mice (**Figure 2D**). These lineage tracing results confirm AT2 cell loss with aging and reveal spontaneous and aberrant differentiation of AT2 cells in HPS mice.

Impaired AT2 cell response after acute influenza injury in HPS mice

To evaluate whether impaired proliferation contributes to AT2 cell loss, we employed an influenza model to evaluate AT2 cell function in the context of regeneration after injury (**Figure 3A**) (19, 20). Because AT2 cell loss occurred in HPS1, HPS2, and HPS1/2 mice but with less marked of an AT2 cell transdifferentiation defect was seen in HPS1 and HPS2 mice compared to double mutant HPS1/2 mice, we utilized AT2 cells from HPS1 and HPS2 mice for the subsequent proliferation studies. Weight change and oxygen saturation decreased comparably in WT, HPS1, and HPS2 mice during the first 10

days post-infection (dpi) with H1N1 PR8 influenza; subsequently, oxygen saturations trended lower in HPS1 and HPS2 mice though no mortality was observed in any group (**Figure 3B, C**). Given the heterogeneous nature of influenza-induced lung injury and to ensure appropriate quantification and comparison, a computational image analysis approach was used to cluster image pixels based on H&E staining to define three regions: severely injured, mildly injured, and unaffected (**Figure 3D**). There was no significant difference in the percentages of these regions or in the area formed by keratin 5 (KRT5)-expressing cells across all groups at 14 dpi (**Supplemental Figure 6A-D**). To examine epithelial regeneration after acute influenza infection, we quantified the percentage of EdU^+, proSP-C^+ cells in HPS1 and HPS2 mice relative to WT in severely injured and mildly injured regions at 14 dpi (**Figure 3E-G**). There was a significant decrease in the percentage of proliferating AT2 cells in HPS1 and HPS2 mice compared to WT in severely injured regions, with a 6.4 ± 4.5% decrease in EdU^+, proSP-C^+ cells in HPS1 mice (adjusted $p = .0033$) and a 21.2 ± 3.7% decrease in HPS2 mice (adjusted $p < .0001$) (**Figure 3E, F**). In mildly injured regions, there was a 8.3 ± 3.0% reduction in EdU^+, proSP-C^+ cells in HPS1 mice (adjusted $p = .0012$) and a 10.8 ± 5.3% decrease in HPS2 mice (adjusted $p = .011$) compared to WT (**Figure 3E, G**). Overall, these data demonstrate impaired HPS AT2 cell regeneration in the setting of acute influenza injury.

Intrinsic HPS AT2 cell proliferation defect ex vivo and in vivo

To evaluate whether this impaired HPS AT2 cell proliferation was due to cell intrinsic defects in progenitor function and proliferative capacity, we employed an *ex vivo* organoid model (20). We generated lung organoids with WT primary outgrowth lung fibroblasts and AT2 cells from WT, HPS1, and HPS2 mice at 8 weeks of age (**Figure 4A**). Compared to lung organoids generated with WT AT2 cells, those with HPS2 AT2 cells were significantly smaller in size (adjusted $p = 0.002$) and displayed significantly decreased colony-forming efficiency (CFE) over 21 days of culture at 2.5 ± 0.4% compared to 4.2 ± 0.4% in WT organoids (adjusted $p = .043$) (**Figure 4B-E**). In contrast, organoids generated from

HPS1 AT2 cells demonstrated comparable size and growth compared to those generated with WT AT2 cells (**Figure 4B-E**).

To evaluate intrinsic AT2 cell proliferative capacity *in vivo*, we administered an epithelial cell-specific mitogen, keratinocyte growth factor (KGF), to WT, HPS1, and HPS2 mice at 7 to 9 weeks of age and quantified the percentage of EdU^+, proSP-C^+ cells 48 hours after KGF administration (**Figure 4F**). The percentage of proliferating AT2 cells was significantly reduced in HPS1 (14.2% EdU^+, proSP-C^+ cells, adjusted $p < .0001$) and HPS2 mice (20.9 ± 4.5% EdU^+, proSP-C^+ cells, adjusted $p = 0.001$) compared to WT (29.9 ± 4.6% EdU^+, proSP-C^+ cells) (**Figure 4G, H**). Low rates of AT2 cell proliferation were observed in WT, HPS1, and HPS2 mice administered vehicle (**Figure 4H**). Overall, these data demonstrate an intrinsic proliferative defect in HPS AT2 cells *ex vivo* and *in vivo*.

Transcriptomic signatures of senescence and aberrant AT2 cell differentiation are enriched in HPS AT2 cells

Given the aberrant transdifferentiation and reduced proliferation exhibited by HPS AT2 cells, we sought to identify pathways that could underlie impaired AT2 cell progenitor function and connect them with mechanisms known to drive pulmonary fibrosis. We examined the transcriptomes of AT2 cells isolated from WT, HPS1, HPS2, and HPS1/2 mice at 8 weeks of age. Fluorescence activated cell sorting (FACS) of AT2 cells revealed a significant decrease in the percentage of AT2 cells captured from HPS mice compared to WT (**Supplemental Figure 7A-D**). Differential gene expression testing and over-representation analysis (ORA) demonstrated upregulation of genes associated with immune cell activation and cell cycle regulation in HPS AT2 cells (**Supplemental Figure 8A-I**). HPS1/2 AT2 cells displayed decreased expression of canonical markers of AT2 cells, increased expression of AT1 cell markers, as well an increase in expression of genes associated with a reprogramed transitional cell state, including *Krt8*, *Cldn4*, and *Lgals3* (**Figure 5A**) (21-23). These observations prompted us to examine markers of p53 signaling and cellular senescence, including *Trp53*, *Cdkn1a*, *Cdkn2d*, and *Ccnd1*, which were upregulated in HPS1, HPS2, and HPS1/2 AT2 cells, with the greatest change in expression seen in

HPS1/2 AT2 cells (**Figure 5A, B**) (24-26). In addition, 5.9 ± 1.8% of AT2 cells isolated from HPS1/2 mice at 48 weeks of age stained positive for β-galactosidase, a marker for senescent cells, whereas β-galactosidase activity was not detected in AT2 cells from WT or HPS mice at 8 weeks of age or WT, HPS1, or HPS2 mice at 48 weeks of age (p = .005) (**Figure 5C, D**).

HPS AT2 cells are primed to enter a p53-mediated Krt8^{+} reprogrammed transitional cell state, which persist in HPS1/2 mice and in lung tissue from a patient with HPS-1

With the aberrant transdifferentiation exhibited by HPS AT2 cells and transcriptomic evidence of a reprogrammed transitional cell state, we sought to identify this cell state *in situ*. Lineage-labeled EYFP^{+} cells co-expressing markers of a reprogrammed transitional cell state, including KRT8, CLDN4, and LGALS3, were present in HPS1/2 Sftpc$^{CreERT2/+}$;R26R$^{EYFP/+}$ mice starting at 8 weeks and accumulating through 24 weeks of age (**Figure 6A**, **Supplemental Figure 9A**). These cells were not detected in WT Sftpc$^{CreERT2/+}$;R26R$^{EYFP/+}$ mice, nor were they identified in single mutant HPS1 and HPS2 Sftpc$^{CreERT2/+}$;R26R$^{EYFP/+}$ mice at 8 or 24 weeks of age (**Figure 6A, Supplemental Figure 9A, B**).

To further investigate the dynamics of AT2 cell transdifferentiation and of this Krt8^{+} reprogrammed transitional cell state in HPS1/2 mice, we utilized an *in vitro* feeder-free alveolosphere culture system to evaluate cell intrinsic differentiation (**Figure 6B**) (27, 28). Alveolospheres were generated with AT2 cells from WT or HPS1/2 mice, producing AT1 cells as indicated by AGER staining (**Figure 6C, D**). Upon induction of differentiation, *Krt8*, *Cldn4*, and *Hopx* expression increased across all groups. Expression of *Krt8* and *Hopx* was significantly higher in HPS1/2 alveolospheres compared to WT on day 7 and continued to be significantly upregulated compared to WT on day 14 (**Figure 6E**). As transcriptomic data suggested this aberrant differentiation could be driven by p53-mediated senescence, alveolospheres were treated with PFTα, a p53 inhibitor, during induction of differentiation. Treatment with PFTα decreased *Krt8* and *Hopx* expression in HPS1/2 alveolospheres on day 7 and day 14 of culture to levels comparable to those in WT alveolospheres (**Figure 6E**).

Finally, explanted lung tissue from a patient with HPS-1 pulmonary fibrosis revealed KRT8-expressing cells which co-expressed an epithelial cell marker, NKX2.1 (**Figure 6F**). A subset of these KRT8$^+$, NKX2.1$^+$ cells also expressed HTII-280, a human AT2 cell marker. These KRT8$^+$ epithelial cells were not identified in lung tissue from an age-matched and sex-matched control donor patient (**Figure 6F**). Taken together, these results demonstrate that HPS AT2 cells are primed to transdifferentiate and persist in a Krt8$^+$ reprogrammed transitional cell state, which can be ameliorated *in vitro* in HPS1/2 mice by inhibiting the activity of p53.

Discussion

AT2 cell dysfunction appears to play a central role in disease pathogenesis across sporadic and genetic forms of pulmonary fibrosis. However, the precise mechanisms by which AT2 cell dysfunction drives the fibrotic response in HPS-PF are incompletely understood, and there has been debate about whether mechanisms in HPS-PF are distinct from other heritable forms of pulmonary fibrosis and IPF (1, 2). In this study, we demonstrate that alveolar epithelial maintenance is disrupted in HPS with overall loss of AT2 cells with aging in the setting of AT2 cell progenitor dysfunction. We found evidence of aberrant transdifferentiation and impaired AT2 cell proliferation in the single mutant HPS1 and HPS2 models and the double mutant HPS1/2 model. HPS AT2 cells displayed increased expression of genes associated with a reprogrammed transitional cell state as well as p53-mediated senescence. Lineage tracing and alveolosphere culture studies demonstrated that AT2 cells from HPS1/2 mice appear primed to transdifferentiate and persist in a Krt8$^+$ reprogrammed transitional cell state in a p53-mediated manner. Finally, we demonstrate the presence of KRT8$^+$ epithelial cells in lung tissue from a patient with HPS-1. These findings provide insight into how intrinsic AT2 cell dysfunction contributes to fibrotic remodeling in HPS-PF and highlight shared mechanisms of disease between HPS-PF and other forms of pulmonary fibrosis.

In adults, AT2-to-AT1 cell transdifferentiation is typically observed in the setting of injury, as a subset of progenitor cells are mobilized to regenerate the alveolar epithelium (20, 29). This process occurs

at very low rates during homeostasis, with an approximate turnover rate of 0.005% of the alveolar surface with new AT2 cell-derived AT1 cells per day (30). Several signaling pathways have been implicated as regulators of AT2 cell transdifferentiation, including Wnt/β-catenin, BMP, TGF-β, and p53 (31-33). Evidence to support the role of aberrant transdifferentiation of AT2 cells in pulmonary fibrosis first came from studies utilizing bleomycin and lipopolysaccharide (LPS) injury models, with the identification of epithelial cell subpopulations enriched in expression of *Krt8*, *Cldn4*, and *Lgals3* (21-23). These cells, which have been referred to as pre-alveolar type 1 transitional cell state (PATS), damage-association transition progenitors (DATPs), and Krt8^{+} alveolar differentiation intermediates (ADIs), appear to result from incomplete transdifferentiation of AT2 cells into AT1 cells (21-23). In HPS, through lineage tracing and alveolosphere studies without exogenous stimuli, we now provide the first data revealing that AT2 cells from single mutant HPS1 and HPS2 mice and double mutant HPS1/2 mice display aberrant transdifferentiation, with AT2-derived AT1 cells seen across all HPS models, without detection of this process in WT mice by 24 weeks of age. Notably, we captured the emergence of a Krt8^{+} reprogrammed transitional cell state only in HPS1/2 mice, underscoring their potential role in fibrotic remodeling. Our data further supports emerging evidence that this state may not necessarily be "transitional" in the sense that cells retain their capacity to differentiate into AT1 cells. For some cells, entry into this state may be unidirectional, resulting in loss of the ability to contribute to functional alveolar epithelial maintenance and repair (34).

Given the widespread and nonselective injury induced by bleomycin and LPS, the contribution of other cell types and potential AT1 cell dysfunction in driving aberrant AT2 cell transdifferentiation and the emergence of the Krt8^{+} reprogrammed transitional cell state has been debated (35). In subsequent studies, this cell state has been identified in genetic models with selective AT2 cell modification, including models of accelerated senescence of AT2 cells via *Trp53* activation, surfactant metabolism dysfunction (*Sftpc*^{C185G} mice), and Nkx2.1 ablation in alveolar epithelial progenitors (24, 36, 37). Here, in a feeder-free alveolosphere culture system with only AT2 cells and no stromal support cells, HPS AT2 cells appear primed to transdifferentiate and persist in this Krt8^{+} reprogrammed transitional cell state.

Taken together, this suggests that aberrant transdifferentiation in HPS is driven by intrinsic AT2 cell dysfunction, although other cell types may provide additional feedback to further drive this process (34).

In addition to aberrant transdifferentiation, HPS AT2 cell progenitor dysfunction also appears to manifest with impaired proliferation. Under homeostatic conditions, AT2 cells are largely quiescent yet some degree of proliferation is required to maintain the alveolar epithelium (38). Other models have demonstrated that interruption of AT2 cell proliferative capacity contributes to fibrotic remodeling (24, 39). Both rare and common variants in *KIF15*, a kinesin involved in regulation of mitosis, increase risk for IPF, and *KIF15* expression is decreased in replicating lung epithelial cells in patients with IPF (39). We observed decreased rates of proliferation in HPS AT2 cells in a lung organoid model and in two *in vivo* models, after mitogenic stimulation and with an influenza injury model. This impaired proliferation may result from not only depletion of the AT2 cell progenitor pool, but also decreased proliferative capacity of these progenitor cells. Notably, HPS1 AT2 cells appeared to perform comparably to WT AT2 cells in an organoid model but exhibited impaired proliferation after administration of KGF and after injury in an influenza model. This may reflect differences in the consequences of the HPS1 and HPS2 mutations on AT2 cell function as well as the models utilized to study cell proliferation and regeneration. Furthermore, differences in AT2 cell proliferation rates after acute influenza infection by injury severity suggests that the HPS mutations have divergent effects on AT2 cell subpopulations, particularly those that function as progenitor cells (20, 40).

In the setting of impaired progenitor function and the progression of AT2 cell loss with aging, transcriptomic analyses highlighted a role for p53-mediated senescence in driving AT2 cell dysfunction and pulmonary fibrosis in HPS. From the study of telomere disorders, accelerated senescence of AT2 cells has long been implicated in pulmonary fibrosis (41). In an experimental murine model, conditional loss of function of SIN3 transcription regulator homolog A (*Sin3a*), a regulator of Trp53 acetylation, in AT2 cells induced senescence, impaired proliferation, and caused loss of AT2 cells, resulting in spontaneous, progressive fibrosis. Mice with loss of function of both *Sin3a* and p53 did not exhibit AT2 cell loss and did not develop significant fibrosis, indicating that activation of the p53 pathway is

necessary to induce AT2 cell senescence and fibrosis (24). While some reports suggest that p53 is necessary for complete AT2-to-AT1 cell differentiation in the setting of acute injury, the role of this pathway may be context- and disease-dependent, as ectopic activation can be deleterious (22, 32, 42). Previous studies of the Krt8^{+} transitional reprogrammed cell state have demonstrated that these cells show increased expression of genes involved in p53, DNA damage, and cellular senescence pathways (22, 24, 34). Indeed, inhibition of p53 was sufficient to attenuate upregulation of *Krt8* and *Hopx* in alveolospheres generated with HPS1/2 AT2 cells compared to WT, suggesting that p53-mediated senescence is the driver of aberrant differentiation and this transitional cell state in HPS.

Although increased apoptosis of AT2 cells has been observed across many forms of pulmonary fibrosis, there remains debate about whether depletion of AT2 cells is necessary or sufficient to drive fibrotic remodeling (2, 7, 43, 44). In contrast to *Sin3a* loss of function mice, selective ablation of AT2 cells via activation of diphtheria toxin resulted in significant AT2 cell loss without the development of significant fibrosis (24). Although previous studies have described increased AT2 cell apoptosis in HPS1/2 mice as well as bleomycin-challenged but not naïve HPS1 and HPS2 mice, we did not observe AT2 cell apoptosis in any of the HPS models up to 48 weeks of age (13, 15). This may have resulted from differences in techniques and assays used to evaluate apoptosis, and we cannot rule out that increased cell death may contribute to AT2 cell loss, in addition to defective proliferation and aberrant differentiation. Regardless, these data suggest that progenitor dysfunction and accelerated senescence of AT2 cells are mechanisms capable of driving fibrotic remodeling, rather than AT2 cell loss alone.

Senescent cells, via the senescence-associated secretory phenotype (SASP), are thought to produce cytokines, chemokines, and growth factors, which activate immune cells and fibroblasts, promoting fibrotic remodeling (45). p53 activation in AT2 cells has been shown to promote myofibroblast differentiation via TGF-β signaling (42). In addition, global *Krt8* knockout mice exhibited decreased macrophage recruitment after bleomycin injury, with significantly lower levels of monocyte chemoattractant protein-1 (MCP-1/CCL2), a SASP factor, in bronchoalveolar lavage (BAL) fluid (34). Our previous findings in HPS AT2 cells are consistent with these models (10, 46, 47). Prior studies

demonstrated that HPS AT2 cells have excess production of monocyte MCP-1, a SASP factor, and epithelial-specific deletion of MCP-1 reduced fibrotic susceptibility in HPS mice (17, 46). HPS-1 patients have also been shown to have elevated levels of MCP-1 in bronchoalveolar lavage (BAL) fluid that correlate with lung disease severity (48). Additional studies are required to evaluate the secretome of HPS AT2 cells, as well as further examine interactions between AT2 cells, macrophages, and fibroblasts, to identify which factors drive fibrotic remodeling in HPS.

The mechanisms by which the HPS endosomal trafficking mutations result in activation of the p53 pathway and accelerated senescence in AT2 cells are unknown. Unlike findings in telomere disorders and familial IPF, telomere shortening has not been observed in peripheral blood mononuclear cells of individuals with HPS (49). While the HPS mutations could produce cell cycle defects that directly result in cell cycle arrest, it is also possible that they contribute to other forms of cellular dysfunction, including mitochondrial dysfunction and aberrant autophagy, which can induce cellular senescence (11, 14). As these mechanisms have been implicated in other fibrotic lung diseases, there may be interconnecting pathways contributing to AT2 cell senescence in HPS. In mice, there may be an additive effect of the HPS1 and HPS2 mutations that results in markedly impaired progenitor cell function and accelerated senescence with the emergence of a Krt8^{+} reprogrammed transitional cell state in double mutant HPS1/2 AT2 cells. This could underlie the divergent phenotypes observed, with fibrotic sensitivity in HPS1 and HPS2 mice in comparison to the development of spontaneous, progressive fibrosis in HPS1/2 mice. It is important to note, however, that patients only bear single variants, either in *HPS1* or *HPS2.* The emergence of KRT8^{+} epithelial cells and spontaneous pulmonary fibrosis in human HPS patients is likely to result from the combined effects of genetic and environmental factors on AT2 cell function.

As a monogenic disorder with murine models that recapitulate key features of the disease, HPS presents a unique opportunity for the study of progressive pulmonary fibrosis. Our findings provide insight into the role of intrinsic AT2 cell dysfunction in the pathogenesis of pulmonary fibrosis in HPS, suggesting common mechanisms, including dysregulated AT2 cell progenitor function with impaired proliferation and aberrant transdifferentiation, driving the fibrotic response in sporadic and genetic forms

of pulmonary fibrosis. The relative contributions of rare and common genetic risk variants, in conjunction with environmental exposures, may vary across different forms of pulmonary fibrosis, but it is likely that these pathways converge, resulting in failure to maintain alveolar epithelial integrity. Understanding the mechanisms that drive AT2 cell transdifferentiation in HPS-PF and the optimal method to modulate the p53 pathway to promote epithelial maintenance and repair and prevent fibrotic remodeling will be critical. Additional studies at single-cell resolution may enable further characterization of the subpopulations of epithelial cells in HPS. We also found features of functional divergence between HPS1 and HPS2 AT2 cells in an organoid model and an influenza injury model, highlighting that the differences exist between HPS subtypes that may help illuminate key aspects of HPS biology. Given the shared pathways that have been identified, further study of the role of alveolar epithelial dysfunction in HPS-PF should have broad applicability across genetic and sporadic fibrotic lung diseases.

Methods

Animal studies and treatment

Naturally occurring HPS1, HPS2, and HPS3 mice, which harbor mutations in the mouse homologues of the *HPS1*, *AP3B1*, and *HPS3* genes, respectively, were maintained on the C57BL6/J background (50). Transgenic HPS2 (HPS2 TG) mice, with partial correction of AP3b1 in the lung epithelium driven by human-SFTPC promoter, as described previously (10). Double mutant HPS1/2 mice were generated by mating homozygous HPS1 and homozygous HPS2 mice (16, 18, 51). WT Sftpc$^{CreERT2/+}$;R26R$^{EYFP/+}$ (Jackson Laboratory, strain # 006148) mice were provided by Dr. David Frank and generated by Dr. Harold Chapman (University of California, San Francisco) as described previously, and bred with HPS1, HPS2, and HPS1/2 mice to generate HPS1 Sftpc$^{CreERT2/+}$;R26R$^{EYFP/+}$, HPS2 Sftpc$^{CreERT2/+}$;R26R$^{EYFP/+}$, and HPS1/2 Sftpc$^{CreERT2/+}$;R26R$^{EYFP/+}$ mice, respectively (52). Both male and female mice were utilized, as fibrosis occurs equally in patients with HPS of both sexes. 4- to 48-week-old animals were used for experiments, as specified. For lineage trace experiments, four-week-old Sftpc$^{CreERT2/+}$;R26R$^{EYFP/+}$ mice were administered tamoxifen (200 mg/kg body weight) in corn oil via oral gavage for three consecutive days. Keratinocyte growth factor (KGF) was obtained as palifermin (Amgen). KGF dissolved in vehicle (PBS) at a dose of 5 mg/kg or vehicle alone was administrated via intratracheal injection 48 hours prior to euthanasia and isolation of lungs (53). For cell proliferation experiments, pulse-chase 5-ethynyl-2'-deoxyuridine (EdU) dissolved in filtered PBS was administered via intraperitoneal injection at a dose of 50 mg/kg four hours prior to euthanasia and isolation of lungs.

Human lung tissue

Normal lung samples were obtained through the University of Pennsylvania Lung Biology Institute's Human Lung Tissue Bank. These samples were obtained from de-identified non-used lungs donated for organ transplantation through an established protocol (PROPEL, approved by University of Pennsylvania Institutional Review Board) with informed consent in accordance with institutional and NIH procedures, and consent was provided by next of kin or healthcare proxy (54). HPS-1 patient tissue samples were

obtained through the University of Pennsylvania as part of the Prospective Registry of Outcomes in Patients Electing Lung Transplantation (PROPEL) (Penn cohort) (54). The patient was diagnosed based on genetic testing. The University of Pennsylvania Institutional Review Board approved this study, and written informed consent was obtained. All patient information was removed before use.

Histology and immunofluorescence

Lungs were harvested at a constant pressure of 30 cm H_2O and were fixed overnight at 4°C in 4% paraformaldehyde (PFA). For whole-mount imaging, lung tissue was washed in PBS, embedded in 4% low-melting agarose, and sectioned at 150 µm thickness. For paraffin embedding, lung tissue was washed in PBS, dehydrated in a graded series of ethanol washes, embedded in paraffin wax, and sectioned at 7 µm thickness. For human tissue, tissue was cut from the distal regions of the human lungs. 2 cm by 2 cm pieces of peripheral parenchyma were washed five times in cold PBS and then placed in 2% PFA overnight. The tissue was washed with PBS and dehydrated to 100% ethanol over the subsequent 12 to 24 hours, paraffin embedded and then sectioned at a thickness of 8 µm. Hematoxylin and eosin (H&E) and Masson's trichrome staining were performed according to standard procedures. Immunofluorescence (IF) staining was performed with antibodies for prosurfactant protein-C (proSP-C) (Invitrogen, PA5-71680), NKX2.1 (Invitrogen, MA5-13961), GFP (Abcam, ab6673), LAMP3 (Synaptic Systems, 391 005), AGER (R&D Systems, MAB1179), KRT8 (DSHB), CLDN4 (Invitrogen, PA5-32354), LGALS3 (Invitrogen, 14-5301-82), and HTII-280 (Terrace Biotech). EdU staining was performed with the Click-iT EdU cell proliferation kit according to the manufacturer's instructions (Invitrogen). Terminal deoxynucleotidyl transferase dUTP nick end labeling (TUNEL) staining was performed using TUNEL assay apoptosis detection kit per the manufacturer's instructions (Biotium). Slides were mounted in Vectashield Antifade Mounting Medium (Vector Labs). Images were captured using a Leica confocal microscope. All image quantification was performed on serial confocal images from z-stack max intensity composites. For quantification, 10 images per sample were randomly selected via the 405 nm (DAPI)

channel. Manual counting of DAPI nuclei, proSP-C$^+$ cells, NKX2.1$^+$ cells, and EYFP$^+$ cells was performed in a blinded fashion.

Alveolar epithelial type II cell isolation

Murine lung single cell suspensions were prepared by dispase digestion (55). Briefly, dispase (50 U/mL) was instilled in lungs followed by agarose to ensure digestion of distal airspaces and prevent incorporation of epithelial cells from distal airways. Lungs were incubated in a dispase solution for 45 minutes at room temperature, then DNase I (Stem Cell) was added, and lungs were teased apart with forceps. Serial filtration through 70-µm and 40-µm cell strainers was performed to create a single cell suspension, followed by ACK lysis to remove red blood cells. AT2 cells were subsequently isolated by fluorescence activated cell sorting (FACS) using antibodies for cell surface markers via negative selection for CD45, positive selection for EpCAM, and negative selection for β4 integrin (CD104) (Biolegend) (19, 52). Samples of the AT2 cell suspensions were fixed and stained for proSP-C, with confirmation of purity > 95%.

Lung organoid assays

AT2 cells were isolated as described above. Live cell numbers were verified using a hemocytometer and Trypan Blue solution. In each technical replicate, 5,000 AT2 cells were combined with 50,000 primary outgrowth WT murine lung fibroblasts in 50% Matrigel (growth factor reduced, phenol-red free) (Corning) and in small airway growth media (Lonza) with the following additives: insulin, transferrin, bovine pituitary extract, retinoic acid, and gentamicin (all from Lonza), with cholera toxin (Sigma) and FBS (Corning). The ROCK inhibitor thiazovivin (Stem Cell) was included in the media for the first two days and media was changed every 2 to 3 days. Images were captured over the course of culture using a Leica Thunder microscope. Images were processed in ImageJ with thresholding and then binarized. All organoids within a well were used for quantification. Organoid number and size were quantified using the analyze particles function in ImageJ with a cutoff of 1500 µm^2. Colony forming efficiency was calculated

by dividing the organoid number by the number of input AT2 cells (5,000). Organoids were fixed and stained with antibodies for proSP-C (Invitrogen, PA5-71680) and AGER (Rage) (R&D Systems, MAB1179).

Influenza infection

H1N1 PR8 influenza virus was generously provided by Dr. Andrew Vaughan (University of Pennsylvania) and titration by $TCID_{50}$ for infectivity was performed in MDCK cells (56). For AT2 cell proliferation studies, we performed an initial set of experiments with WT and HPS2 mice, aged 8 to 12-weeks. Mice were anesthetized with 4% isoflurane in 100% O_2 via an anesthesia vaporizer system and H1N1 PR8 influenza was delivered intratracheally at a dose of 100 U diluted in 50 µl PBS. In a subsequent experiment, HPS1 and WT mice, aged 8 to 12-weeks, were anesthetized with xylazine and ketamine via intraperitoneal injection, and H1N1 PR8 influenza was delivered intranasally at a dose of 100 U diluted in 50 µl PBS. For weight and oxygen saturation measurements, a subsequent cohort of WT, HPS1, and HPS2 mice, aged 8 to 12-weeks, were also anesthetized with xylazine and ketamine via intraperitoneal injection, and H1N1 PR8 influenza was delivered intranasally at a dose of 100 U diluted in 50 µl PBS. Mouse weights were tracked daily starting from the day of infection. Mice were shaved and pulse oximetry measurements were obtained using MouseOx Plus (Starr Life Sciences) every second or third day starting from the day of infection for the time points noted.

Lung injury assessment

To define regions of lung injury after influenza infection, an unbiased image classification machine learning model was used on H&E-stained sections to cluster image pixels by staining intensity, similar to previously described methodology (20, 40). Three regions of injury were defined: severely injured, mildly injured, and unaffected.

Bulk mRNA sequencing

Total RNA was extracted from freshly isolated AT2 cells using the RNeasy Micro Kit (Qiagen) and stored at -80°C. Frozen total RNA was sent to Genewiz/Azenta Life Sciences (NJ, USA) for bulk mRNA-sequencing, using their standard RNA-seq service. Reads in FASTQ format were aligned to the NCBI mouse genome (mm10/GRCm38) and quantified at the gene level using the nf-core/rnaseq v3.8.1 Nextflow pipeline (57, 58). Differential gene expression analysis was performed using DESeq2 and scanpy (59, 60). Aggregate gene set scores were calculated using the JASMINE scoring metric (61).

β-galactosidase staining

AT2 cells were isolated as described above. AT2 cells were deposited on glass slides by cytospin centrifugation at 500 rpm for 5 minutes. Fixation and staining were performed using a β-galactosidase staining kit per the manufacturer's instructions at pH 6.0 (Cell Signaling). Cells were counterstained with DAPI to enable quantification.

Alveolosphere differentiation assay

Alveolosphere culture was performed as previously described (27, 28). AT2 cells were isolated as described above. Live cell numbers were verified using a hemocytometer and Trypan Blue solution. In each technical replicate, 7,000 AT2 cells were plated in 50% Matrigel (growth factor reduced, phenol-red free) (Corning). Alveolospheres were cultured in alveolar maintenance media with IL-1β and the ROCK inhibitor Y-27632 (Sigma) for the first four days, alveolar differentiation media for the next four days, then transitioned to alveolar maintenance media for the remaining six days in culture. Media was changed every 2 to 3 days. Pifithrin-α (PFTα) was added to the alveolar differentiation media at a concentration of 30 μM (62, 63). Organoids were fixed and stained with antibodies for LAMP3 (Synaptic Systems, 391 005) and AGER (Rage) (R&D Systems, MAB1179).

Quantitative polymerase chain reaction

Alveolospheres were dissociated from Matrigel using Cell Recovery Solution (Corning). RNA was isolated from alveolospheres using Direct-zol RNA Microprep Kits (Zymo). Complementary DNA (cDNA) was synthesized from total RNA using High-Capacity cDNA Reverse Transcription Kits (Applied Biosystems). Quantitative polymerase chain reaction (qPCR) was performed using the TaqMan system (Applied Biosystems). qPCR primers are listed in **Supplemental Table 1**. Relative gene expression was calculated using the ΔΔCt method (64).

Picrosirius red staining

Staining for collagen was performed using picrosirius red staining kit per the manufacturer's instructions (Polysciences Inc.). Digital morphometric measurements and collagen quantitation were performed as previously described (65). WT lung tissue was normalized to a collagen area of 3.0%.

Statistics

Statistical analyses were performed with GraphPad Prism. Student's t-test were used for comparison between groups for parametric data and Mann-Whitney U-test for non-parametric data. Results are presented as mean ± SEM. p values < .05 were considered significant. For multiple comparisons, the Benjamini-Hochberg procedure was utilized with a false discovery rate of 0.05. Adjusted p values < .05 were considered significant.

Study approval

All procedures for animal experiments were performed under the guidance of and in compliance with all ethical regulations of the Children's Hospital of Philadelphia Institutional Animal Care and Use Committee (IACUC). Human HPS-1 specimens were obtained from the NDRI at the time of lung transplantation under established protocols. The normal human donor samples used were from de-identified, non-used lungs donated for research (PROPEL) with approval of the University of

Pennsylvania Institutional Review Board (IRB) and in accordance with NIH procedures (54). Informed consent was provided by next of kin or health care proxy.

Data availability

Mouse AT2 cell bulk RNA sequencing data are available in the NCBI's public functional genomics data repository Gene Expression Omnibus. Values for all data points in graphs are reported in the Supporting Data Values file.

Grant funding: J.Y.W. received support through an NIH Ruth L. Kirschstein National Research Service Award Institutional Research Training Grant (2-T32-HL-007586-36). J.A.Z. receives support through an NIH Pathway to Independence Award (R00-HL141684), an NIH Maximizing Investigators' Research Award (R35-GM146835), and an ATS/Hermansky-Pudlak Syndrome Network Research Grant. D.B.F receives support through an NIH Mentored Clinical Scientist Research Career Development Award (K08-HL140129). L.R.Y. receives support through an NIH Research Project Grant (R01-HL119503), an NIH Midcareer Investigator Award in Patient-Oriented Research (K24-HL143281), and the Rare Lung Diseases Frontier Program at the Children's Hospital of Philadelphia.

Author contributions: J.Y.W. designed and performed experiments, analyzed and interpreted the data, and wrote and edited the manuscript. N.S.M. analyzed and interpreted the data and edited the manuscript. S.S. designed and performed experiments and edited the manuscript. B.J.B. designed experiments and edited the manuscript. S.M.L., M.C.B., and E.C. provided access to human samples and assisted with tissue processing. J.B.K. designed experiments and provided access to human samples and assisted with tissue processing. J.A.Z. and D.B.F. designed experiments, interpreted the data, and edited the manuscript. L.R.Y. designed the study, interpreted the data, and wrote and edited the manuscript.

Acknowledgements: We thank the participating patients for providing human lung tissue specimens. We would also like to thank Ruby Pan, Mary Kate Goldy, and Heather Kelley for technical assistance and Dr. Andrew Vaughan, Dr. Luis Rodriguez, and Dr. Michael Beers for experimental guidance.

References

1. Parimon T, Yao C, Stripp BR, et al. Alveolar epithelial type II cells as drivers of lung fibrosis in idiopathic pulmonary fibrosis. International journal of molecular sciences. 2020;21(7):2269.

2. Katzen J, Beers MF. Contributions of alveolar epithelial cell quality control to pulmonary fibrosis. J Clin Invest. 2020;130(10):5088-99.

3. Selman M, Pardo A. The leading role of epithelial cells in the pathogenesis of idiopathic pulmonary fibrosis. Cell Signal. 2020;66:109482.

4. Lawson WE, Crossno PF, Polosukhin VV, et al. Endoplasmic reticulum stress in alveolar epithelial cells is prominent in IPF: Association with altered surfactant protein processing and herpesvirus infection. American Journal of Physiology-Lung Cellular and Molecular Physiology. 2008;294(6):L1119-26.

5. Armanios MY, Chen JJ, Cogan JD, et al. Telomerase mutations in families with idiopathic pulmonary fibrosis. N Engl J Med. 2007;356(13):1317-26.

6. Katzen J, Wagner BD, Venosa A, et al. An SFTPC BRICHOS mutant links epithelial ER stress and spontaneous lung fibrosis. JCI insight. 2019;4(6)

7. Korfei M, Ruppert C, Mahavadi P, et al. Epithelial endoplasmic reticulum stress and apoptosis in sporadic idiopathic pulmonary fibrosis. American journal of respiratory and critical care medicine. 2008;178(8):838-46.

8. Bueno M, Lai Y, Romero Y, et al. PINK1 deficiency impairs mitochondrial homeostasis and promotes lung fibrosis. J Clin Invest. 2015;125(2):521-38.

9. Hengst M, Naehrlich L, Mahavadi P, et al. Hermansky-Pudlak syndrome type 2 manifests with fibrosing lung disease early in childhood. Orphanet journal of rare diseases. 2018;13(1):1-11.

10. Young LR, Gulleman PM, Bridges JP, et al. The alveolar epithelium determines susceptibility to lung fibrosis in Hermansky-Pudlak syndrome. American journal of respiratory and critical care medicine. 2012;186(10):1014-24.

11. Ahuja S, Knudsen L, Chillappagari S, et al. MAP1LC3B overexpression protects against Hermansky-Pudlak syndrome type-1-induced defective autophagy in vitro. American Journal of Physiology-Lung Cellular and Molecular Physiology. 2016;310(6):L519-31.

12. Cuevas-Mora K, Roque W, Shaghaghi H, et al. Hermansky-Pudlak syndrome-2 alters mitochondrial homeostasis in the alveolar epithelium of the lung. Respiratory research. 2021;22(1):1-11.

13. Zhou Y, He CH, Herzog EL, et al. Chitinase 3–like–1 and its receptors in Hermansky-Pudlak syndrome–associated lung disease. J Clin Invest. 2015;125(8):3178-92.

14. Cinar R, Park JK, Zawatsky CN, et al. CB1R and iNOS are distinct players promoting pulmonary fibrosis in Hermansky–Pudlak syndrome. Clinical and Translational Medicine. 2021;11(7):e471.

15. Young LR, Pasula R, Gulleman PM, et al. Susceptibility of Hermansky-Pudlak mice to bleomycin-induced type II cell apoptosis and fibrosis. American journal of respiratory cell and molecular biology. 2007;37(1):67-74.

16. Mahavadi P, Korfei M, Henneke I, et al. Epithelial stress and apoptosis underlie Hermansky-Pudlak syndrome–associated interstitial pneumonia. American journal of respiratory and critical care medicine. 2010;182(2):207-19.

17. Atochina-Vasserman EN, Bates SR, et al. Early alveolar epithelial dysfunction promotes lung inflammation in a mouse model of Hermansky-Pudlak syndrome. American journal of respiratory and critical care medicine. 2011;184(4):449-58.

18. Lyerla TA, Rusiniak ME, Borchers M, et al. Aberrant lung structure, composition, and function in a murine model of Hermansky-Pudlak syndrome. American Journal of Physiology-Lung Cellular and Molecular Physiology. 2003;285(3):L643-53.

19. Vaughan AE, Brumwell AN, Xi Y, et al. Lineage-negative progenitors mobilize to regenerate lung epithelium after major injury. Nature. 2015;517(7536):621-5.

20. Zacharias WJ, Frank DB, Zepp JA, et al. Regeneration of the lung alveolus by an evolutionarily conserved epithelial progenitor. Nature. 2018;555(7695):251-5.

21. Strunz M, Simon LM, Ansari M, et al. Alveolar regeneration through a Krt8 transitional stem cell state that persists in human lung fibrosis. Nature communications. 2020;11(1):1-20.

22. Kobayashi Y, Tata A, Konkimalla A, et al. Persistence of a regeneration-associated, transitional alveolar epithelial cell state in pulmonary fibrosis. Nat Cell Biol. 2020;22(8):934-46.

23. Choi J, Park J, Tsagkogeorga G, et al. Inflammatory signals induce AT2 cell-derived damage-associated transient progenitors that mediate alveolar regeneration. Cell stem cell. 2020;27(3):366,382. e7.

24. Yao C, Guan X, Carraro G, et al. Senescence of alveolar type 2 cells drives progressive pulmonary fibrosis. American Journal of Respiratory and Critical Care Medicine. 2021;203(6):707-17.

25. Parimon T, Chen P, Stripp BR, et al. Senescence of alveolar epithelial progenitor cells: A critical driver of lung fibrosis. American Journal of Physiology-Cell Physiology. 2023;325(2):C483-95.

26. Hamsanathan S, Alder JK, Sellares J, et al. Cellular senescence: The trojan horse in chronic lung diseases. American journal of respiratory cell and molecular biology. 2019;61(1):21-30.

27. Katsura H, Sontake V, Tata A, et al. Human lung stem cell-based alveolospheres provide insights into SARS-CoV-2-mediated interferon responses and pneumocyte dysfunction. Cell stem cell. 2020;27(6):890,904. e8.

28. Konishi S, Tata A, Tata PR. Defined conditions for long-term expansion of murine and human alveolar epithelial stem cells in three-dimensional cultures. STAR protocols. 2022;3(2):101447.

29. Nabhan AN, Brownfield DG, Harbury PB, et al. Single-cell wnt signaling niches maintain stemness of alveolar type 2 cells. Science. 2018;359(6380):1118-23.

30. Jansing NL, McClendon J, Henson PM, et al. Unbiased quantitation of alveolar type II to alveolar type I cell transdifferentiation during repair after lung injury in mice. American journal of respiratory cell and molecular biology. 2017;57(5):519-26.

31. Aspal M, Zemans RL. Mechanisms of ATII-to-ATI cell differentiation during lung regeneration. International Journal of Molecular Sciences. 2020;21(9):3188.

32. Kaiser AM, Gatto A, Hanson KJ, et al. p53 governs an AT1 differentiation programme in lung cancer suppression. Nature. 2023;619(7971):851-9.

33. Jiang P, Gil de Rubio R, Hrycaj SM, et al. Ineffectual type 2–to–type 1 alveolar epithelial cell differentiation in idiopathic pulmonary fibrosis: Persistence of the KRT8hi transitional state. American journal of respiratory and critical care medicine. 2020;201(11):1443-7.

34. Wang F, Ting C, Riemondy KA, et al. Regulation of epithelial transitional states in murine and human pulmonary fibrosis. J Clin Invest. 2023;133(22)

35. Konkimalla A, Konishi S, Macadlo L, et al. Transitional cell states sculpt tissue topology during lung regeneration. Cell Stem Cell. 2023;30(11):1486,1502. e9.

36. Katzen J, Rodriguez L, Tomer Y, et al. Disruption of proteostasis causes IRE1 mediated reprogramming of alveolar epithelial cells. Proceedings of the National Academy of Sciences. 2022;119(43):e2123187119.

37. Toth A, Kannan P, Snowball J, et al. Alveolar epithelial progenitor cells require Nkx2-1 to maintain progenitor-specific epigenomic state during lung homeostasis and regeneration. Nature Communications. 2023;14(1):8452.

38. Barkauskas CE, Cronce MJ, Rackley CR, et al. Type 2 alveolar cells are stem cells in adult lung. J Clin Invest. 2013;123(7):3025-36.

39. Zhang D, Povysil G, Kobeissy PH, et al. Rare and common variants in KIF15 contribute to genetic risk of idiopathic pulmonary fibrosis. American journal of respiratory and critical care medicine. 2022;206(1):56-69.

40. Liberti DC, Kremp MM, Liberti III WA, et al. Alveolar epithelial cell fate is maintained in a spatially restricted manner to promote lung regeneration after acute injury. Cell reports. 2021;35(6):109092.

41. Alder JK, Barkauskas CE, Limjunyawong N, et al. Telomere dysfunction causes alveolar stem cell failure. Proceedings of the National Academy of Sciences. 2015;112(16):5099-104.

42. Enomoto Y, Katsura H, Fujimura T, et al. Autocrine TGF-β-positive feedback in profibrotic AT2-lineage cells plays a crucial role in non-inflammatory lung fibrogenesis. Nature Communications. 2023;14(1):4956.

43. Flaherty KR, Travis WD, Colby TV, et al. Histopathologic variability in usual and nonspecific interstitial pneumonias. American journal of respiratory and critical care medicine. 2001;164(9):1722-7.

44. Thannickal VJ, Horowitz JC. Evolving concepts of apoptosis in idiopathic pulmonary fibrosis. Proceedings of the American Thoracic Society. 2006;3(4):350-6.

45. Schafer MJ, White TA, Iijima K, et al. Cellular senescence mediates fibrotic pulmonary disease. Nature communications. 2017;8(1):1-11.

46. Young LR, Gulleman PM, Short CW, et al. Epithelial-macrophage interactions determine pulmonary fibrosis susceptibility in Hermansky-Pudlak syndrome. JCI insight. 2016;1(17)

47. Young LR, Borchers MT, Allen HL, et al. Lung-restricted macrophage activation in the pearl mouse model of Hermansky-Pudlak syndrome. The Journal of Immunology. 2006;176(7):4361-8.

48. Rouhani FN, Brantly ML, Markello TC, et al. Alveolar macrophage dysregulation in Hermansky-Pudlak syndrome type 1. American journal of respiratory and critical care medicine. 2009;180(11):1114-21.

49. Gochuico BR, Dorward H, Franklin T, O'Brien K, et al. Shortened Telomeres in Type II Alveolar Epithelial Cells in Hermansky-Pudlak Syndrome Pulmonary Fibrosis In: C59. GENETIC AND EPIGENETIC MECHANISMS IN PULMONARY FIBROSIS.. American Thoracic Society; 2019 p. A5267.

50. Li W, Rusiniak ME, Chintala S, et al. Murine Hermansky–Pudlak syndrome genes: Regulators of lysosome-related organelles. Bioessays. 2004;26(6):616-28.

51. Guttentag SH, Akhtar A, Tao J, et al. Defective surfactant secretion in a mouse model of Hermansky-Pudlak syndrome. American journal of respiratory cell and molecular biology. 2005;33(1):14-21.

52. Chapman HA, Li X, Alexander JP, et al. Integrin α6β4 identifies an adult distal lung epithelial population with regenerative potential in mice. J Clin Invest. 2011;121(7):2855-62.

53. Yano T, Mason RJ, Pan T, et al. KGF regulates pulmonary epithelial proliferation and surfactant protein gene expression in adult rat lung. American Journal of Physiology-Lung Cellular and Molecular Physiology. 2000;279(6):L1146-58.

54. Diamond JM, Lee JC, Kawut SM, et al. Clinical risk factors for primary graft dysfunction after lung transplantation. American journal of respiratory and critical care medicine. 2013;187(5):527-34.

55. Sinha M, Lowell CA. Isolation of highly pure primary mouse alveolar epithelial type II cells by flow cytometric cell sorting. Bio-protocol. 2016;6(22):e2013.

56. Weiner AI, Zhao G, Zayas HM, et al. ΔNp63 drives dysplastic alveolar remodeling and restricts epithelial plasticity upon severe lung injury. Cell reports. 2022;41(11):111805.

57. Di Tommaso P, Chatzou M, Floden EW, et al. Nextflow enables reproducible computational workflows. Nat Biotechnol. 2017;35(4):316-9.

58. Ewels PA, Peltzer A, Fillinger S, et al. The nf-core framework for community-curated bioinformatics pipelines. Nat Biotechnol. 2020;38(3):276-8.

59. Love MI, Huber W, Anders S. Moderated estimation of fold change and dispersion for RNA-seq data with DESeq2. Genome Biol. 2014;15(12):1-21.

60. Wolf FA, Angerer P, Theis FJ. SCANPY: Large-scale single-cell gene expression data analysis. Genome Biol. 2018;19:1-5.

61. Noureen N, Ye Z, Chen Y, et al. Signature-scoring methods developed for bulk samples are not adequate for cancer single-cell RNA sequencing data. Elife. 2022;11:e71994.

62. Zhu J, Singh M, Selivanova G, et al. Pifithrin-α alters p53 post-translational modifications pattern and differentially inhibits p53 target genes. Scientific reports. 2020;10(1):1049.

63. Sohn D, Graupner V, Neise D, et al. Pifithrin-α protects against DNA damage-induced apoptosis downstream of mitochondria independent of p53. Cell Death & Differentiation. 2009;16(6):869-78.

64. Livak KJ, Schmittgen TD. Analysis of relative gene expression data using real-time quantitative PCR and the $2^{-\Delta\Delta CT}$ method. Methods. 2001;25(4):402-8.

65. Nureki S, Tomer Y, Venosa A, et al. Expression of mutant Sftpc in murine alveolar epithelia drives spontaneous lung fibrosis. J Clin Invest. 2018;128(9):4008-24.

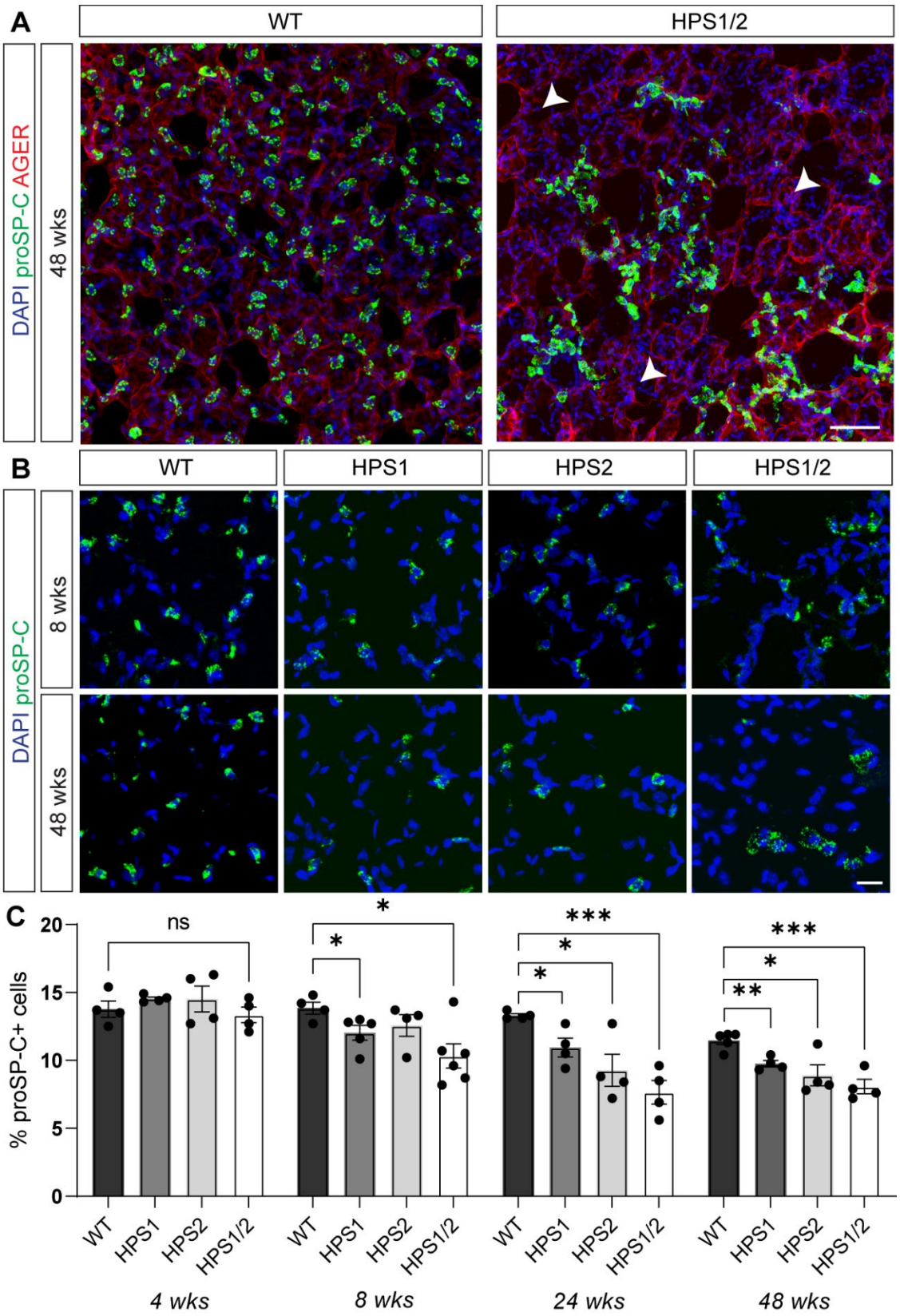

Figure 1. Loss of alveolar type II epithelial (AT2) cells with aging in HPS mice. (A) Representative immunofluorescence (IF) staining of whole-mount lung issue for pro-C and AGER in WT and HPS1/2 mice at 48 weeks of age. Arrows indicate regions of AT2 cell loss. (B) Representative IF staining of paraffin-embedded lung tissue for proSP-C in WT, HPS1, HPS2, and HPS1/2 mice at 8 and 48 weeks of age. (C) Quantification of percentage of proSP-C^{+} cells as a percentage of total cells (by DAPI) in WT, HPS1, HPS2, and HPS1/2 mice at 4, 8, 24, and 48 weeks of age. DAPI stains nuclei (blue). All quantification data are represented as mean ± SEM. Two-tailed t tests: ns, not significant; adjusted * $p < .05$; ** $p < 0.01$, *** $p < .001$; n = 4-6 per group per time point. Scale bars in (A), 50 µm; (B), 20 µm.

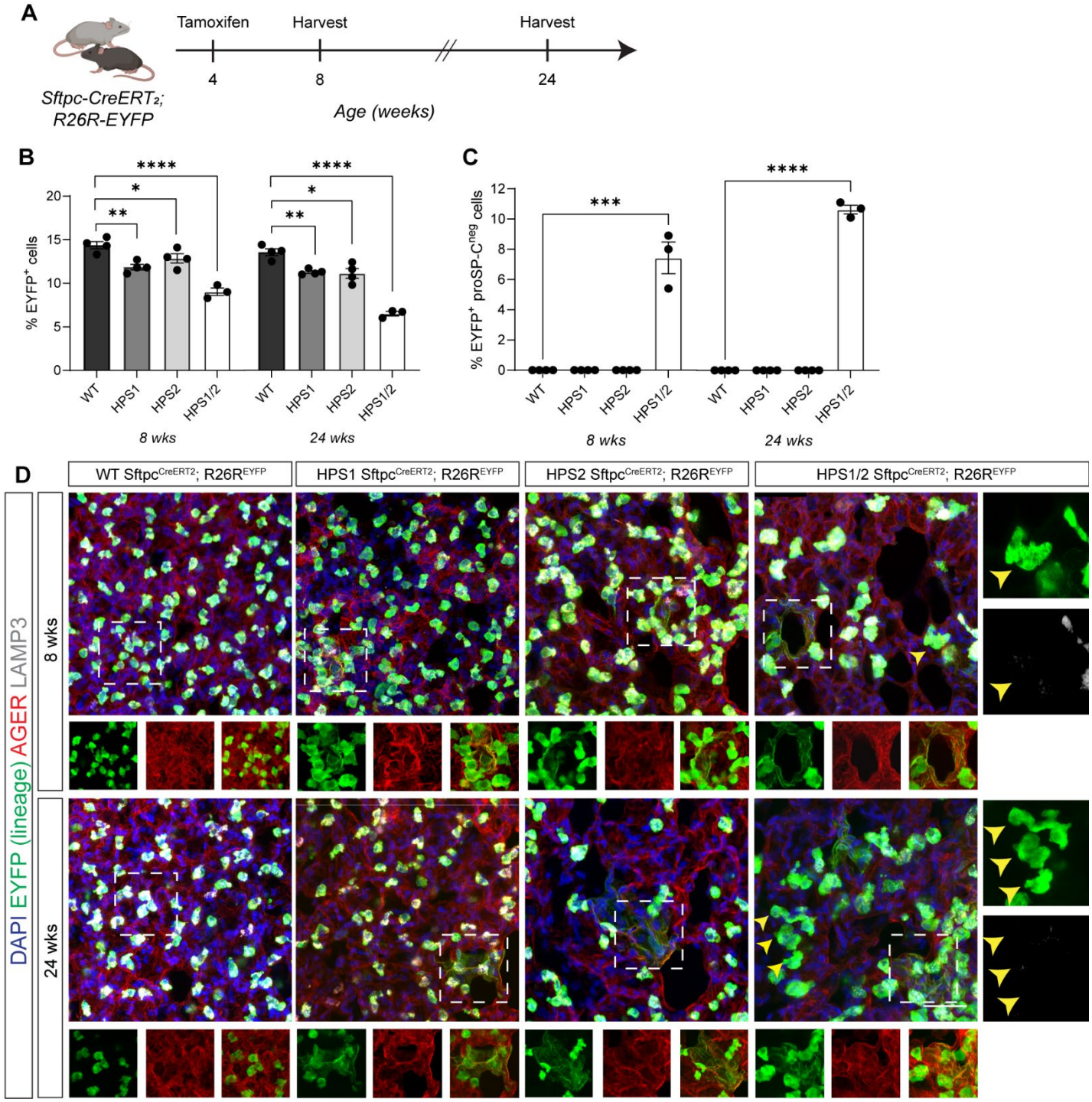

Figure 2. Lineage tracing of alveolar type II epithelial (AT2) cells in HPS mice confirms loss and reveals spontaneous differentiation. A) Schematic to lineage label AT2 cells in WT, HPS1, HPS2, and HPS1/2 Sftpc$^{CreERT2/+}$;R26R$^{EYFP/+}$ mice. (B, C) Quantification of (B) EYFP^{+} cells and (C) EYFP^{+} proSP-C^{neg} cells as a percentage of total cells in WT, HPS1, HPS2, and HPS1/2 Sftpc$^{CreERT2/+}$;R26R$^{EYFP/+}$ mice at 8 and 24 weeks of age. (D) Representative immunofluorescence staining of whole-mount lung tissue for EYFP, AGER, and LAMP3 in WT, HPS1, HPS2, and HPS1/2 Sftpc$^{CreERT2/+}$;R26R$^{EYFP/+}$ mice at 8 and 24 weeks of age. Dashed line boxes represent squamous EYFP^{+}, AGER^{+}, LAMP3^{neg} cells with AGER and EYFP images shown below; arrows indicate cuboidal EYFP^{+}, AGER^{neg}, LAMP3^{neg} cells with magnified EYFP and LAMP3 images shown on the right. DAPI stains nuclei (blue). All quantification data are represented as mean ± SEM. Two-tailed t tests: adjusted * $p < .05$; ** $p < .01$, *** $p < .001$; **** $p < .0001$. n = 3-4 per group per time point. Scale bars in (D), 50 µm. Schematic created with Biorender.com.

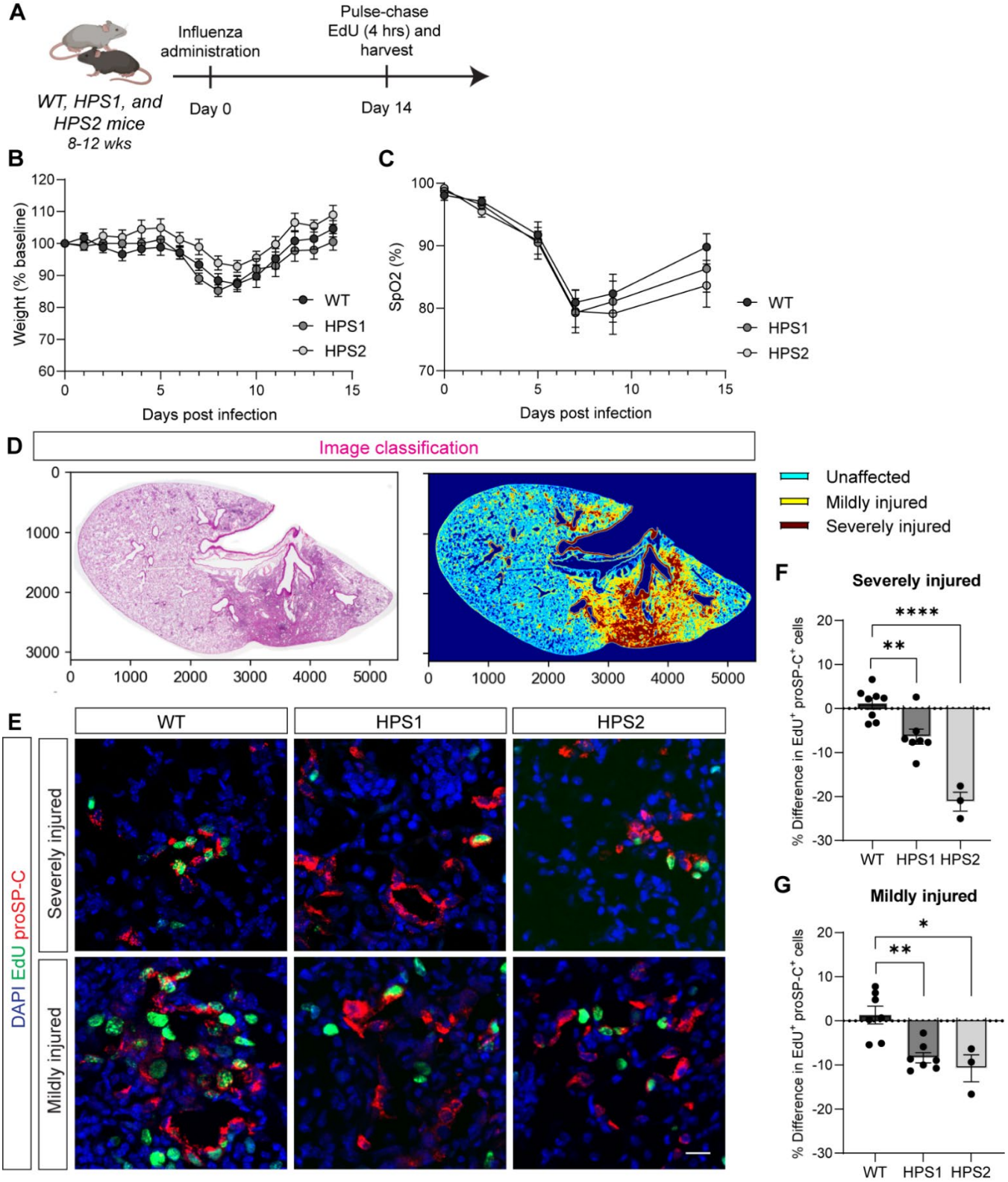

Figure 3. HPS alveolar type II epithelial (AT2) cell response is impaired after acute influenza injury. (A) Schematic of influenza model and EdU pulse-chase in WT, HPS1, and HPS2 mice. (B, C) Mean change in (B) weight and (C) oxygen saturation (SpO_2) in WT, HPS1, and HPS2 mice from 0 to 14 days post infection (dpi). (D) Representative images demonstrating computational image analysis approach to define regions of lung injury from H&E-stained lung sections. (E) Representative immunofluorescence staining of lung tissue for proSP-C and EdU in WT, HPS1, and HPS2 mice at 14 dpi in severely and mildly injured regions. (F, G) Quantification of the percentage difference in EdU-positive AT2 cells (by proSP-C staining) in (F) severely injured and (G) mildly injured regions at 14 dpi in HPS1 and HPS2 mice relative to WT. DAPI stains nuclei (blue). All quantification data are represented as mean ± SEM. Two-tailed t tests: adjusted * $p < .05$, ** $p < .01$, **** $p < .0001$; n = 10 per group in (B, C), n = 6-8 per group in (F), n = 3-4 per group in (G). All scale bars, 20 µm. Schematic created with Biorender.com.

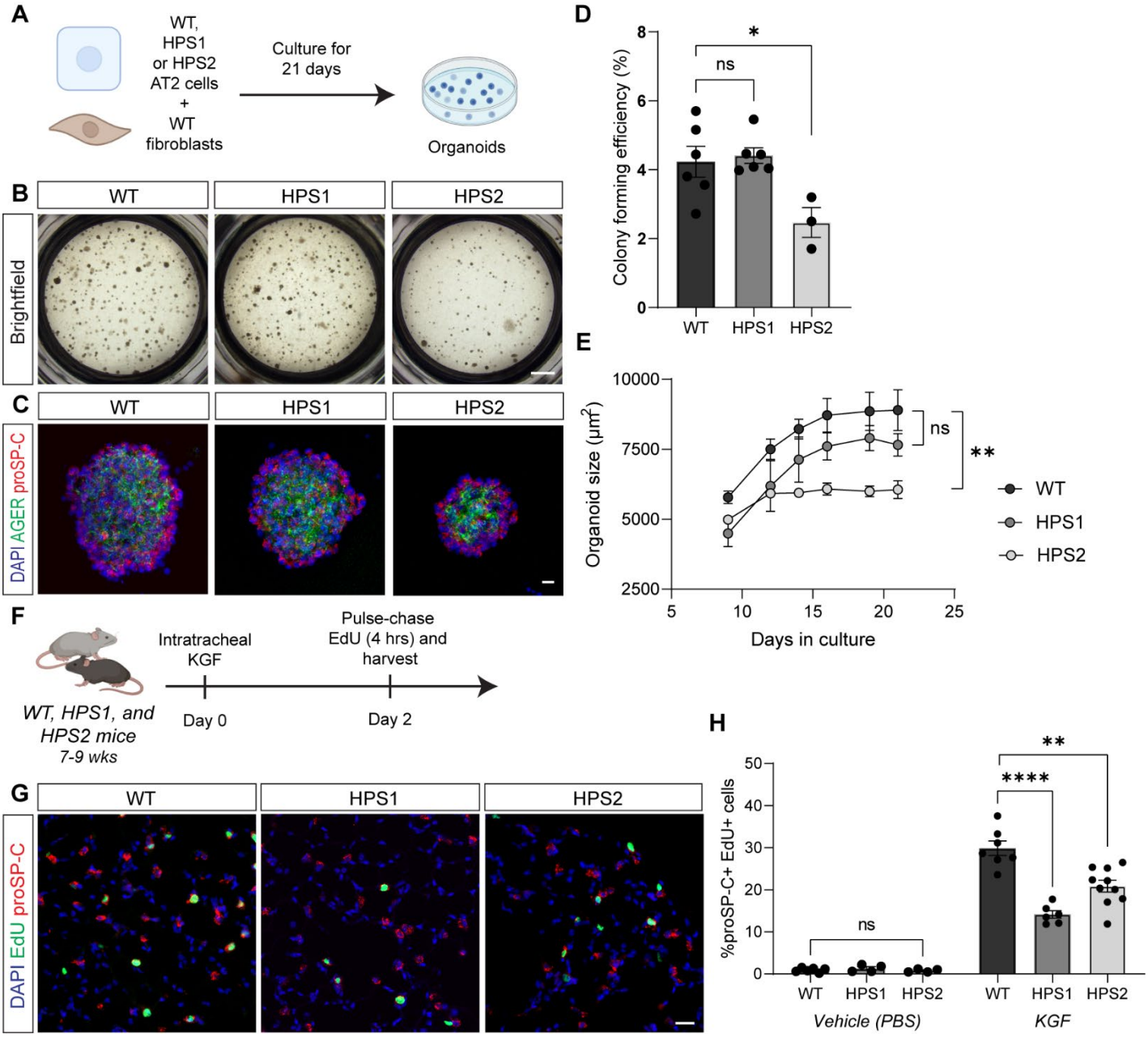

Figure 4. HPS alveolar type II epithelial (AT2) cell proliferation is impaired in an *ex vivo* lung organoid model and after *in vivo* keratinocyte growth factor (KGF) administration. (A) Schematic of lung organoid culture system. (B, C) Representative (B) brightfield imaging and (C) immunofluorescence (IF) staining of lung organoids for AGER and proSP-C generated with AT2 cells isolated from WT, HPS1, or HPS2 mice with WT fibroblasts at day 21 of culture. (D) Quantification of WT, HPS1, and HPS2 organoid size from day 9 to day 21 of culture. (E) Quantification of WT, HPS1, and HPS2 organoid colony forming efficiency (CFE) at day 21 of culture. (F) Schematic of KGF administration and EdU pulse-chase in WT, HPS1, and HPS2 mice. (G) Representative IF staining of lung tissue for proSP-C and EdU in WT, HPS1, and HPS2 mice 48 hours after KGF administration. (H) Quantification of the percentage of EdU-positive AT2 cells (by proSP-C staining) in WT, HPS1, and HPS2 mice 48 hours after vehicle (PBS) and KGF administration. DAPI stains nuclei (blue). All quantification data are represented as mean ± SEM. Two-tailed t tests: ns, not significant; adjusted * $p < .05$, ** $p < .01$, **** $p < .0001$. For (D, E), each point represents the average of at least three replicate wells from one mouse for a total of n = 3-6 mice per group. For (H), n = 4-10 per group per treatment. Scale bars in (B), 1 mm; in (C, G), 20 µm. Schematics created with Biorender.com.

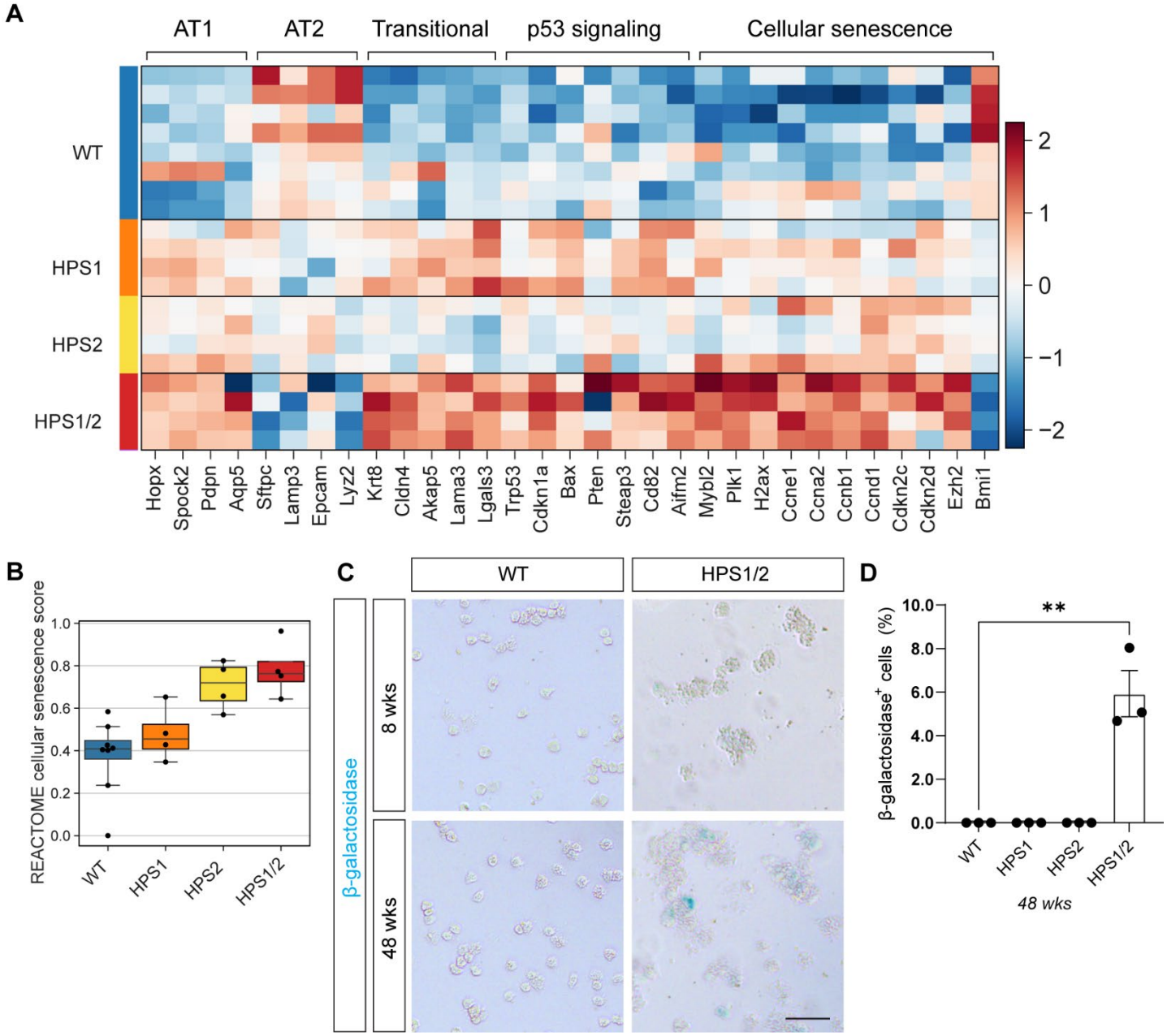

Figure 5. Transcriptomic analysis suggests aberrant transdifferentiation and p53-mediated senescence in HPS alveolar type II epithelial (AT2) cells. (A) Differential expression analysis of AT2, transitional, and AT1 cell genes and p53 signaling pathway and cellular senescence genes in AT2 cells from WT, HPS1, HPS2, and HPS1/2 mice at 8 weeks of age. (B) Overall gene set score for cellular senescence. (C) Representative β-galactosidase staining of AT2 cells isolated from WT and HPS1/2 mice. (D) Quantification of the percentage of β-galactosidase$^+$ cells in WT, HPS1, HPS2, and HPS1/2 mice. DAPI stains nuclei (blue). All quantification data are represented as mean ± SEM. Two-tailed t tests: ** $p < .01$; n = 3-4 per group. Scale bars in (C), 50 µm.

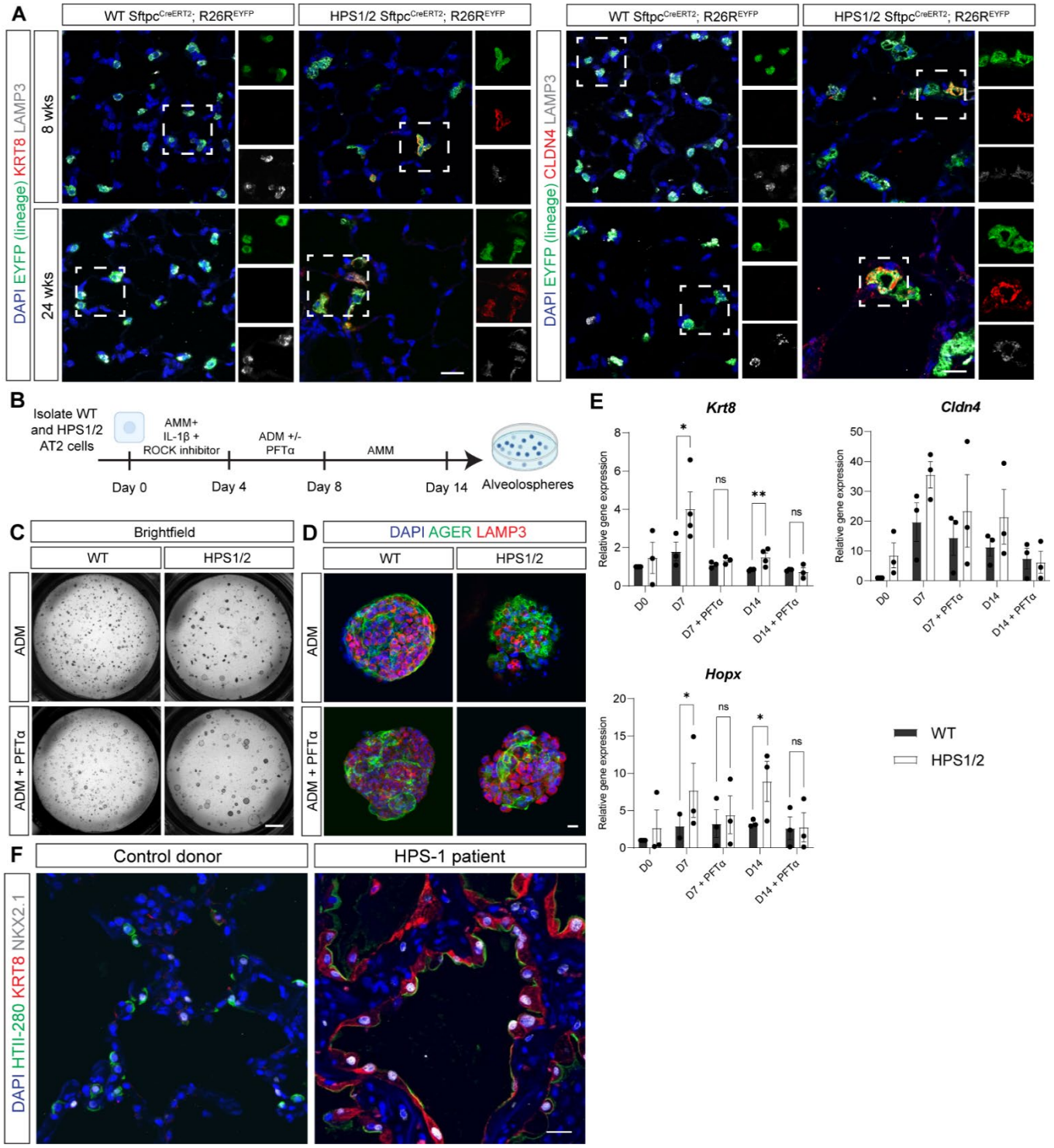

Figure 6. A p53-mediated Krt8^{+} reprogrammed transitional cell state in HPS1/2 mice and Krt8^{+} cells in a patient with HPS-1. (A) Representative immunofluorescence (IF) staining for EYFP, KRT8, CLDN4, and LAMP3 in WT and HPS1/2 Sftpc$^{CreERT2/+}$;R26R$^{EYFP/+}$ mice at 8 and 24 weeks of age. Dashed line boxes represent EYFP^{+} cells with inset boxes displaying EYFP, KRT8 or CLDN4, and LAMP3 staining. (B) Schematic for alveolosphere culture system with alveolar epithelial type II (AT2) cells in alveolar maintenance media (AMM) and alveolar differentiation media (ADM) and treatment with pifithrin-α (PFTα). (C, D) Representative (C) brightfield imaging and (D) IF staining of alveolospheres for AGER and LAMP3 generated with AT2 cells from WT or HPS1/2 mice with and without treatment with PFTα at day 14 (D14) of culture. (E) Relative gene expression of selected reprogrammed transitional cell (*Krt8*, *Cldn4*) and alveolar epithelial type I (AT1) cell (*Hopx*) genes in alveolospheres with and without treatment with PFTα at day 0 (D0), day 7 (D7), and day 14 (D14) of culture. Relative gene expression compared to WT at D0. Each point represents four replicate wells per time point for a total of n = 3-4 mice. (F) Representative IF staining of paraffin-embedded lung tissue from an age- and sex-matched control donor patient and HPS-1 patient for HTII-280, KRT8, and NKX2.1. DAPI stains nuclei (blue). All quantification data are represented as mean ± SEM. Two-tailed t tests: ns, not significant; adjusted * $p < .05$; ** $p < .01$. Scale bars in (A, D, F), 20 µm; (C), 1 mm. Schematic created with Biorender.com.